CFD Analysis of Scale Effects on Conventional and Tip-Modified Propellers

Shin, Keun Woo; Andersen, Poul

Published in:
Proceedings of the Fifth International Symposium on Marine Propulsors - smp'17

Publication date:
2017

Document Version
Peer reviewed version

Fifth International Symposium on Marine Propulsors
smp'17, Espoo, Finland, June 2017

CFD Analysis of Scale Effects on Conventional and Tip-Modified Propellers

Keun Woo Shin[1], Poul Andersen[2]

[1]Propeller & Aftship R&D Department, MAN Diesel & Turbo, Frederikshavn, Denmark
[2]Department of Mechanical Engineering (MEK), Technical University of Denmark (DTU), Kgs.Lyngby, Denmark

ABSTRACT

Full-scale propeller performance is traditionally predicted by scaling model-scale test results, but the traditional scaling methods do not take into account hydrodynamic distinctions of tip-modified propellers in full-scale performance. An open-water CFD analysis is made on scale effects of tip-modified and conventional propellers, which are designed for the same operating condition with identical propeller diameter and expanded area ratio. While model-scale computations are made with a transition model, a fully turbulent flow is modeled in the full-scale computations. The investigation on the effects of the transition model shows that laminar and transitional flow modeling is crucial in model-scale computations. Grid-independent solutions at model and full scale are achieved by grid verification studies.

The CFD analysis of scale effects shows that the efficiency gain of the tip-modified propeller is increased at full scale. The difference of scale effects between the tip-modified and conventional propellers is related to alterations of tip vortex and sectional pressure distributions by the bent tip and the higher spanwise loading at the tip region of the tip-modified propeller.

Keywords

Scale effect, Unconventional propeller, CFD, RANS, Transition model

1 INTRODUCTION

The standard ITTC 1978 scaling method for open-water propeller characteristics adopted by most model test institutes is an extrapolation using Reynolds number-based friction corrections of a representative blade section (ITTC 2008). RANS computations on conventional propellers with different skews and area ratios at model and full scales have shown that ITTC78 scaling method does not reflect larger scale effects for propellers with higher skews and larger area ratios (Krasilnikov et al 2009). Model tests and RANS computations on model-scale low- and high-skew conventional propellers with varying Reynolds number *Rn* have also shown larger scale effects for the high-skew propeller (Funeno 2002).

Tip-modified propellers have been developed to improve propulsive efficiency and to increase lifting-surface span without shortening the clearance from the propeller tip to the hull surface. Nowadays research on tip-modified propellers is active with increased demand for reducing fuel consumption and greenhouse gas emissions in ship operations. Efficiency improvements of tip-modified propellers are made by reducing vortex shedding across the blade tip and redistributing the spanwise blade loading. As the intensity of tip vortex varies from model scale to full scale depending on *Rn*, scale effects on tip-modified propellers are more critical than on conventional propellers.

Two tip-modified propellers and a conventional propeller have been designed for a set of common requirements. Open-water CFD investigations of scale effects on those three propellers by using two different RANS solvers have shown larger scale effects for the tip-modified propellers than for the conventional one (Brown et al 2014). A tip-modified propeller has been retrofitted on a tanker in lieu of an original conventional propeller. Self-propulsion model tests and sea trials on both the propellers have shown slightly larger scale effects on the tip-modified propeller (Andersen et al 2005).

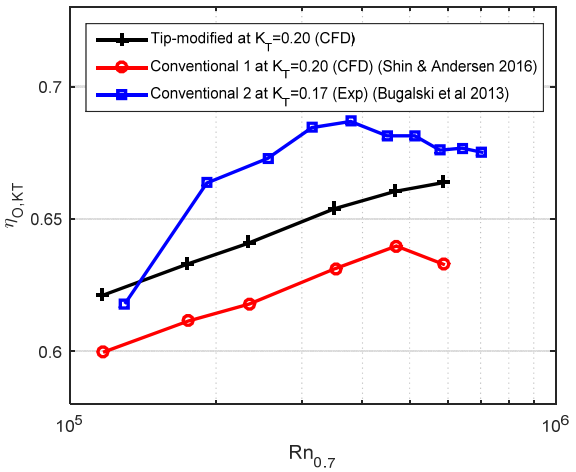

Figure 1: Open-water efficiency $\eta_{O,KT}$ at the design thrust coefficient K_T with respect to $Rn_{0.7}$ from CFD on tip-modified and conventional propellers (Shin & Andersen 2016) and from model tests on another conventional propeller (Bugalski et al 2013)

RANS computations have been made on tip-modified and conventional propellers designed for an identical operating condition with common geometrical parameters at a range of $Rn_{0.7} \approx 10^5 - 10^6$ corresponding to those in self-propulsion and open-water propeller model tests (Shin & Andersen 2016), where

$$Rn_{0.7} = C_{0.7}\frac{\sqrt{(0.7\cdot\pi\cdot D\cdot N)^2+V_A^2}}{\nu} \quad (1)$$

and $C_{0.7}$ is the chord length at $0.7R$, D is the propeller diameter, N is the propeller rate of revolution, V_A is the propeller advance speed and ν is the kinematic viscosity.

Open-water model tests have been made on another conventional propeller with varying $Rn_{0.7}$ (Bugalski et al 2013). As $Rn_{0.7}$ is increased, open-water efficiency $\eta_{O,KT}$ at the design thrust coefficient K_T rises up to a certain point and drops down for the two conventional propellers, as shown in Figure 1. As $\eta_{O,KT}$ for the tip-modified propeller constantly increases within the considered range of $Rn_{0.7}$, scale effects become relatively larger for the tip-modified propeller.

In this research work, the CFD analysis of scale effects on tip-modified and conventional propellers is extended to a higher value of $Rn_{0.7} = 1.3\cdot10^7$ corresponding to full-scale propeller operations. $Rn_{0.7}$ is varied in a range of $Rn_{0.7} \approx 1.8\cdot10^5 - 2.3\cdot10^7$ with keeping a constant Froude number, whereas $Rn_{0.7}$ is increased without conforming to Froude's law in Figure 1. The correlation of scale effects with viscous shear stress, non-viscous pressure and induced drag related to tip vortex is analyzed for both tip-modified and conventional propellers. RANS computations are conducted with and without a transition model to investigate the effects of laminar and transitional flows.

CFD on model-scale propellers is often validated against model test results, but it is hard to find full-scale propeller performance measurements in open-water condition, which can be used for full-scale CFD validations. Therefore, grid independency of CFD results is highlighted for reliable full-scale CFD. Systematic grid verification studies have been made for full-scale hull simulations in bare-hull and self-propulsion conditions (Visonneau et al 2016). Grid independency has been studied by using three structured grids for model- and full-scale open-water propellers (Sanchez-Caja et al 2014). Unstructured grids have shown difficulty to obtain grid-independent results for full-scale propellers (Haimov et al 2011). Grid-independent solutions for model- and full-scale tip-modified propellers with respect to overall grid size and boundary layer flow resolution are attempted by using unstructured grids and improving grid similarity. Grid-independent results for the model-scale propeller are validated against open-water model test results.

2 PROPELLER MODELS

Tip-modified and conventional propellers on a single-screw 35,000 DWT bulk carrier are considered for CFD analysis of scale effects. Both propellers consisting of 4 blades with identical diameter and expanded area ratio of $D_F = 5.9$ m and $A_E/A_O = 0.38$, respectively, are designed for the same operating condition of $V_S = 14$ kn and $N = 91.3$ rpm. The tip-modified propeller is a Kappel propeller characterized by a smoothly curved tip bending towards the suction side of the blade. The comparison of tip rake, spanwise load distribution and other geometrical parameters between two propellers are illustrated in Shin & Andersen (2016). A model propeller of $D_M = 0.25$ m for the tip-modified propeller has been produced and evaluated in open-water and self-propulsion tests in Force Technology, Denmark.

Figure 2: Experimental model (top) of tip-modified propeller and computational models of tip-modified (bottom left) and conventional (bottom right) propeller

3 CFD SETUP

A steady incompressible RANS solver in the commercial CFD package StarCCM+ is adopted with curvature-corrected k-ω SST turbulence model excluding a wall function for CFD simulations. Since laminar and transitional boundary layer flows are formed on a model-scale propeller, γ-Re_θ transition model is also adopted. The effects of laminar and transitional flows on model- and full-scale propellers are investigated by comparing CFD results with and without the transition model.

A single blade is modeled with front hubcap and downstream shaft following the open-water test setup in a quarter-cylinder fluid domain with periodic boundary condition on the sides. The quarter-cylinder domain extends $3\cdot D$ from the propeller plane to the inlet and $6\cdot D$ to the outlet with a radius of $4\cdot D$. A moving reference frame for modeling propeller rotation is applied to an inner domain extending from the propeller plane $0.4\cdot D$ upstream and $2.4\cdot D$ downstream with a radius of $0.6\cdot D$.

Computational grids are generated by unstructured trimmed hexahedral meshing with including prism layers on wall surfaces. The surface mesh size on the overall surface of the blade and hub is $\Delta x_M = 0.5 - 1.0$ mm at model scale and $\Delta x_F = 2.0 - 4.0$ mm at full scale. The grid

size increases twice after 10 layers. The maximum grid size is 7·Δx at the blade tip in Zone 1, 14·Δx around the rotating domain in Zone 2 and 35·Δx in Zone 3, as shown in Figure 3. The grid is refined to 0.5·Δx along the blade edges for resolving high curvature.

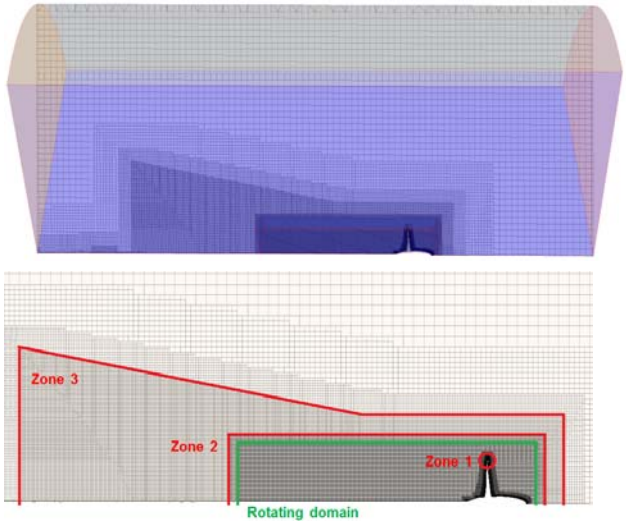

Figure 3: Computational domain and grid on a longitudinal cross section

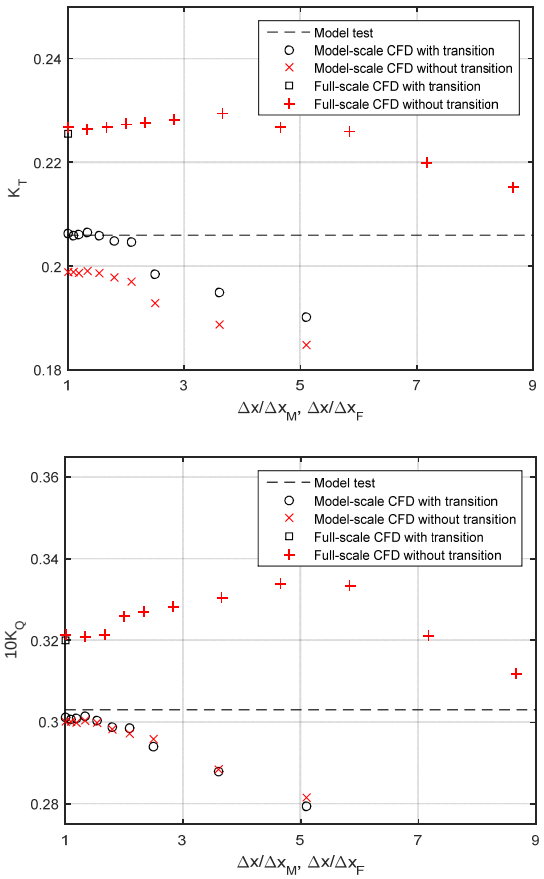

Figure 4: K_T and K_Q as a function of normalized grid size for CFD on tip-modified propeller at model and full scale

The prismatic mesh consists of 9 layers with a total thickness of 0.2 mm at model scale and 0.14 mm at full scale. The first-cell height is Δh_M = 9.6 μm at model scale and Δh_F = 6.5 μm at full scale, which leads mostly to $y+ \leq$ 1. The cell height increases with 1.2 stretching rate in the prism layers.

4 GRID VERIFICATION

A grid verification study is made with respect to Δx and Δh for model- and full-scale computations. Grid similarity is ensured by constant growth rates from the surface mesh to the outer volume mesh and zonal grid sizes defined as functions of Δx. The grid study is conducted only for the tip-modified propeller at the design advance ratio of J = 0.6. The full-scale grid study is made at the actual propeller speed of N = 1.6 rps in the design condition, whereas a higher speed of N = 20.0 rps than N = 7.8 rps scaled by Froude's law is applied to the model-scale grid study in the same way as in the open-water model test.

The full-scale grid study is made without the transition model, because the boundary layer flow on a full-scale propeller is considered to be fully turbulent except for a small region at the leading edge. The model-scale grid study is conducted with and with the transition model. The model-scale grid study with the transition model is looked into first.

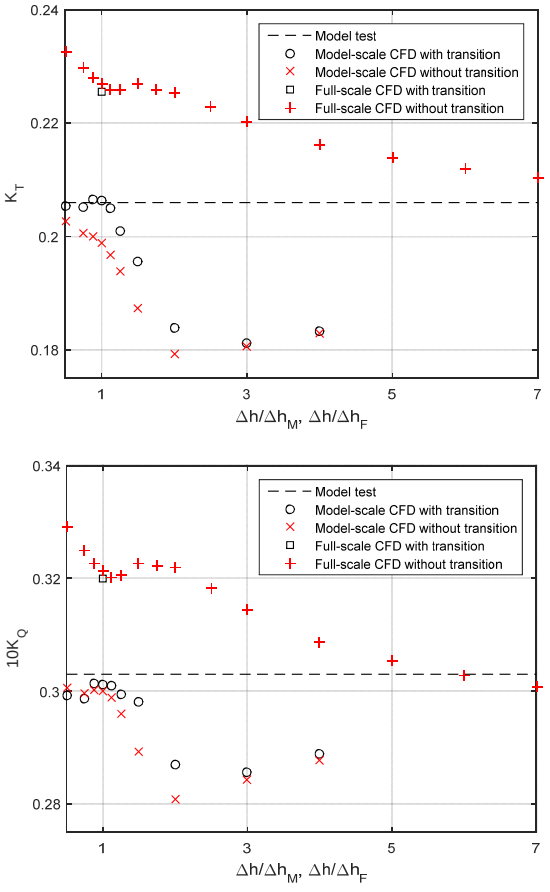

Figure 5: K_T and K_Q as a function of normalized prism-layer thickness for CFD on tip-modified propeller at model and full scale

Δx_M = 0.5 – 1.0 mm and Δh_M = 9.6 μm are adopted for the final model-scale grid after the grid verification study. Figure 4 and 5 show the variations of K_T and K_Q at $\Delta x/\Delta x_1$ = 1.0 – 5.0 and $\Delta h/\Delta h_M$ = 0.5 – 4.0 for model-scale computations. Although a constant convergence rate is

not shown due to unstructured grids, both K_T and K_Q are converged with variances of less than 0.3% at 5 grid sizes of $\Delta x/\Delta x_M$ = 1.0 – 1.55. K_T and K_Q are also converged with respect to $\Delta h/\Delta h_M$ with variances of less than 0.8% at 5 prism-layer thicknesses of $\Delta h/\Delta h_M$ = 0.5 – 1.13, but the variances for $\Delta h/\Delta h_M$ are slightly larger than those for $\Delta x/\Delta x_M$. The converged values of K_T and K_Q are close to K_T = 0.206 and K_Q = 0.303 from the model test with errors of 0.2% and 0.6%, respectively.

Δx_f = 2.0 – 4.0 mm and Δh_F = 6.5 μm are adopted for the final full-scale grid after the grid verification study. While Δx_f of the full-scale grid is 4 times larger than Δx_m of the model-scale grid, $\Delta x_F/D_F$ is about 6 times smaller than $\Delta x_M/D_M$, so the total number of computational cells is 17.8 million for the full-scale computation, which is about 3.5 times higher than 5.2 million for the model-scale computation.

The variations of K_T and K_Q at $\Delta x/\Delta x_F$ = 1.0 – 9.0 and $\Delta h/\Delta h_F$ = 0.5 – 7.0 for full-scale computations are also shown in Figure 4 and 5. Both K_T and K_Q are converged with variances of less than 0.2% for 3 grid sizes of $\Delta x/\Delta x_F$ = 1.0 – 1.7. Although K_T and K_Q are seemingly converged with variances of less than 0.5% for 5 prism-layer thicknesses of $\Delta h/\Delta h_F$ = 1.0 – 1.8, K_T and K_Q continuously increase for smaller prism-layer thicknesses of $\Delta h/\Delta h_F \leq$ 1.0, probably because turbulent boundary layer is unevenly resolved for thinner prism layers. The converged values of K_T and K_Q for full-scale computations are higher than those for model-scale computations by 9.9% and 6.7%, respectively.

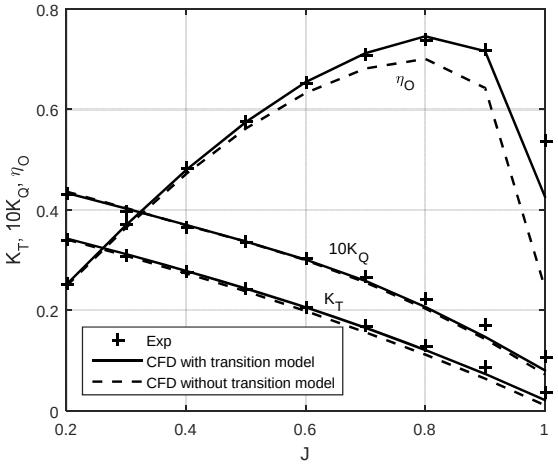

Figure 6: Open-water curves from model test and CFD with and without transition model for tip-modified propeller

5 TRANSITION MODEL

When looking into the model-scale grid study without the transition model, K_T and K_Q are also converged for $\Delta x/\Delta x_M$ and $\Delta h/\Delta h_M$ in a similar way as those with the transition model, as shown in Figure 4 and 5, but K_T is not converged for $\Delta h/\Delta h_M$ and it continuously increases for smaller prism-layer thicknesses of $\Delta h/\Delta h_M \leq 1$. The K_T error of the computations without the transition model from the model test result is significantly increased to 3.5%. The K_Q error is also increased to 1.0%, but the increase is not so much as that of the K_T error.

In Figure 6, the open-water curves from the computations on the final grid with and without the transition model are compared with that from the model test. While the deviations in K_T, K_Q and η_O from the experimental result are within 2% at J = 0.2 - 0.6 for the computations with the transition model, the underestimations of K_T and K_Q become larger at low blade loadings of $J \geq 0.7$. The underestimation of K_T is more pronounced for the computations without the transition model at $J \geq 0.6$, which leads to the underestimation of η_O.

In Figure 7, the surface-constrained streamlines and the skin friction coefficient C_F on the blade surface of both propellers are compared between model-scale computations with and without the transition model on the final grid and a preliminary grid with a lower boundary layer resolution where $y+$ is about twice the value of the final grid, where

$$C_F = \frac{\tau_W}{0.5 \cdot \rho \cdot N^2 \cdot D^2} \quad (2)$$

and τ_W is the wall shear stress.

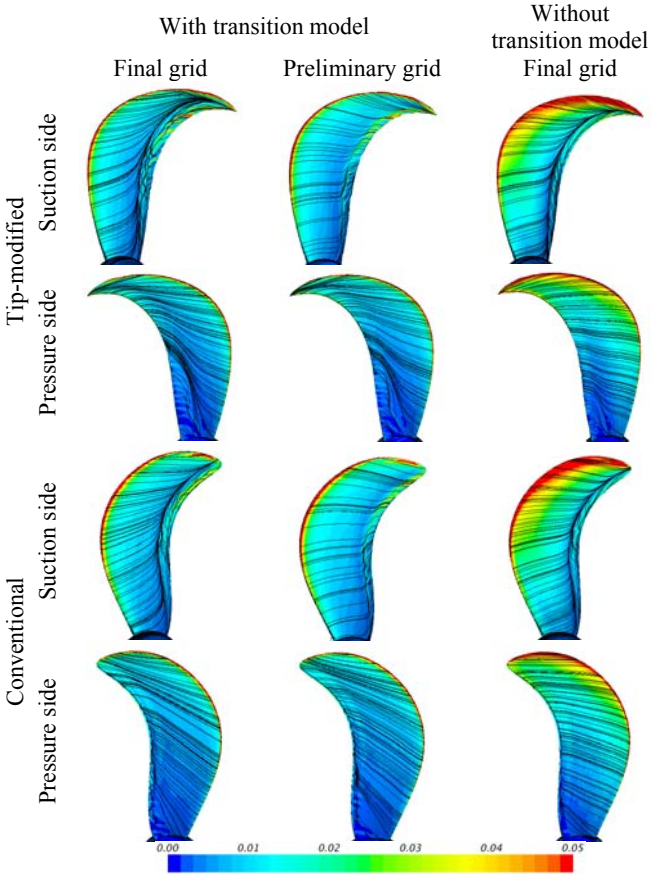

Figure 7: Surface-constrained streamlines and skin friction coefficient from model-scale computations

When comparing the streamlines from the final and preliminary grids, the turbulent flow separation indicated by radially outward deflections of tangential flows on the suction side near the trailing edge is more pronounced for the final grid with about twice higher boundary layer resolution than the preliminary grid. The tangential flow

on the suction side before the flow separation is along rather constant radii for the preliminary grid like that from the computation without the transition model, whereas it is directed slightly upwards for the final grid. The difference of the pressure-side flow is relatively small between the final and preliminary grids because laminar-turbulent transition is more gradual due to the favorable pressure gradient than on the suction side.

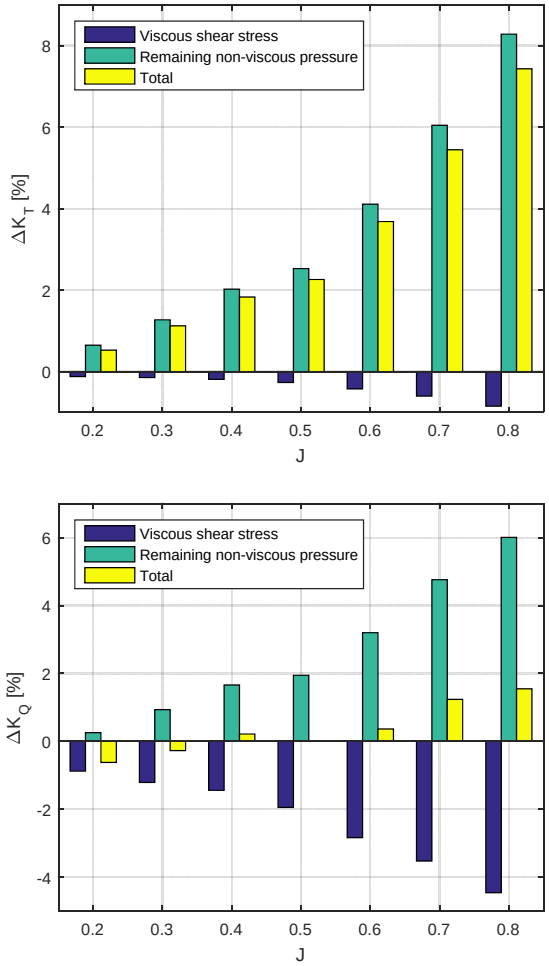

Figure 8: Differences of K_T and K_Q between computations on the tip-modified propeller with and without the transition model ($\Delta\phi = \phi_{Transition} / \phi_{NoTransition} - 1$)

When excluding the transition model, the friction on the overall blade surface increases especially at the leading edge and the flow separation at the trailing edge of the suction side and at inner radii of the pressure side comparatively is reduced, compared to the computation result with the transition model. In Figure 8, K_T and K_Q are compared between the computations on the tip-modified propeller with and without the transition model in a range of $J = 0.2 - 0.8$. K_T from the transition-modeled computation is larger than that from the fully-turbulent flow computation in the whole range of J and ΔK_T increases at higher J, because the thrust increase from non-viscous pressure is larger than the thrust reduction from viscous shear stress and the difference is increased at higher J. When laminar and transitional flows are modeled, the high suction extended to $0.83 \cdot C$ at $0.8 \cdot R$ in Figure 9 can be related to the thrust increase, whereas the suction gradually falls down from about $0.7 \cdot C$ without the transition model. The K_Q difference is up and down within 1.5%, because the torque increase from non-viscous pressure is on a similar level as the torque reduction from viscous shear stress. In Figure 10, vortex flows visualized by an iso-surface of Q-criterion Q = 30,000 show that the tip vortex extent is slightly larger for the computation with the transition model, which leads to larger induced drag from the tip vortex and so it can contribute to the larger torque from non-viscous pressure.

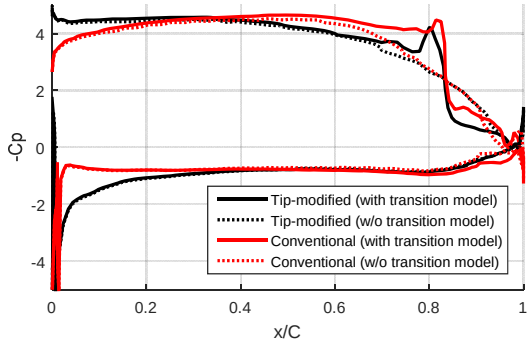

Figure 9: Sectional pressure distribution at $0.8 \cdot R$ ($C_P = (P-P_\infty)/0.5 \cdot \rho \cdot N^2 \cdot D^2$)

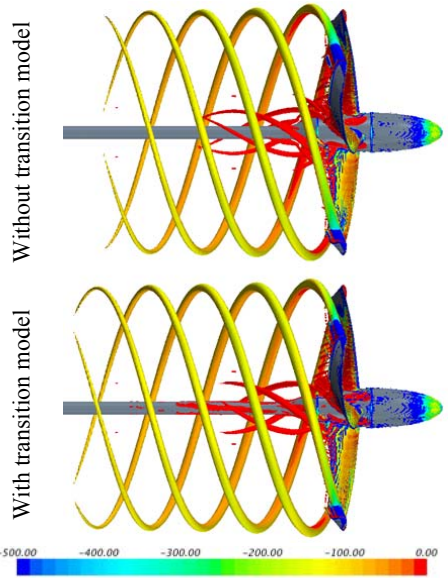

Figure 10: Vortex flows visualized by iso-surfaces of Q-criterion Q = 30,000 with colors indicating the vorticity component around the axial direction on the tip-modified propeller with / without the transition model

A full-scale computation with the transition model is made only for the final grid. The differences of K_T and K_Q are within 0.4% between the full-scale computations with and without the transition model. In Figure 11, the difference in the streamlines is not noticeable between the computations with and without the transition model, whereas C_F is lower at the leading edge of both sides and higher at the mid-chord and the trailing edge of the suction side in the computation with the transition model. As C_F at full scale in Figure 11 is lower than that at model scale in Figure 7, the portion of the torque from viscous shear stress to the total torque is 1.5 – 1.7% in the full-

scale computations, which is smaller than 3.3 – 6.4% in the model-scale computations. It is to be noted that the upper limit of C_F in Figure 7 is 5 times higher than that in Figure 11. The difference in the torque from viscous shear stress between the full-scale computations with and without the transition model is within 0.2% of the total torque, which is also smaller than about 3% in the model-scale computations.

In Figure 11, C_F from the full-scale computation on a preliminary grid of $\Delta x/\Delta x_F = 2$ is lower than that on the final grid. While streamlines are formed smoothly along constant radii for the final grid, it deflects radially outwards at inner radii and some are not smooth for the preliminary grid, which demonstrates that flow separation can occur numerically due to insufficient grid resolution.

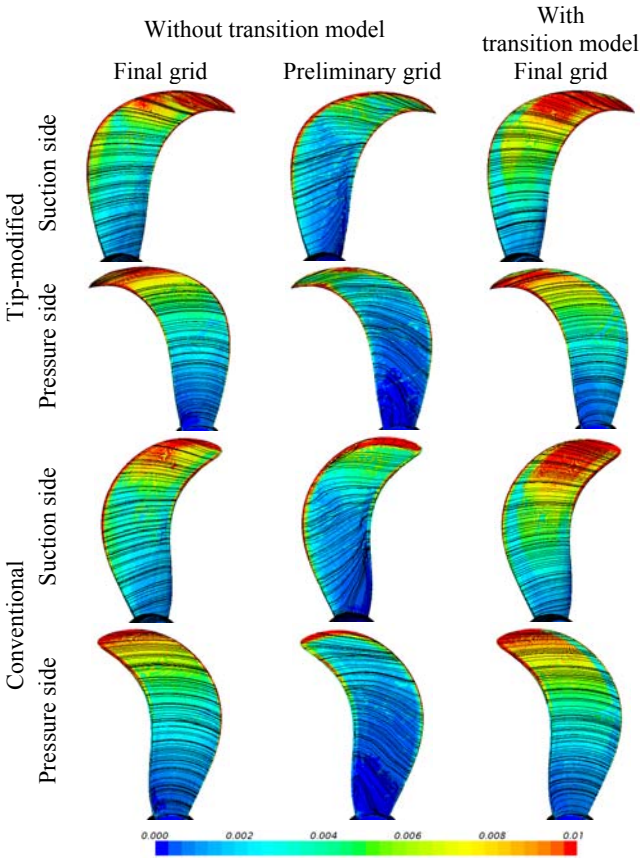

Figure 11: Surface-constrained streamlines and skin friction coefficient from full-scale computations

6 SCALE EFFECT

Computations are made on the tip-modified and conventional propellers at model and full scale by using the final grid from the grid verification study. Laminar to turbulent flow transitions are modeled by adopting the transition model in model-scale computations, whereas a fully turbulent flow is modeled in full-scale computations without the transition model.

In Figure 12, K_T and K_Q at model scale are higher for the tip-modified propeller at the design condition and low loadings of $J \geq 0.6$ and lower at high loadings of $J \leq 0.4$. At full scale, K_T and K_Q for both propellers are increased over the whole considered range of J. Since the increase of K_T is larger than that of K_Q, η_O at full scale is higher than that at model scale.

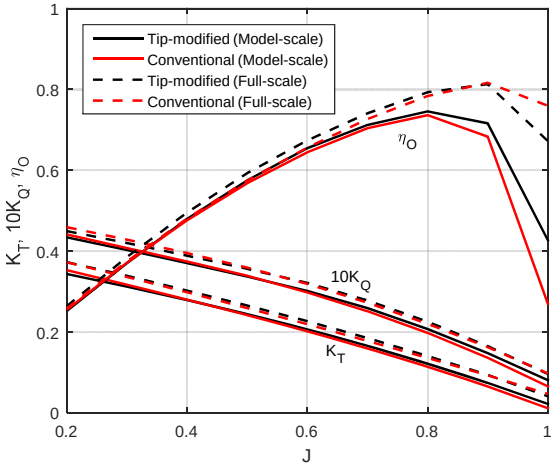

Figure 12: Open-water curves from CFD for the tip-modified and conventional propellers at model and full scales

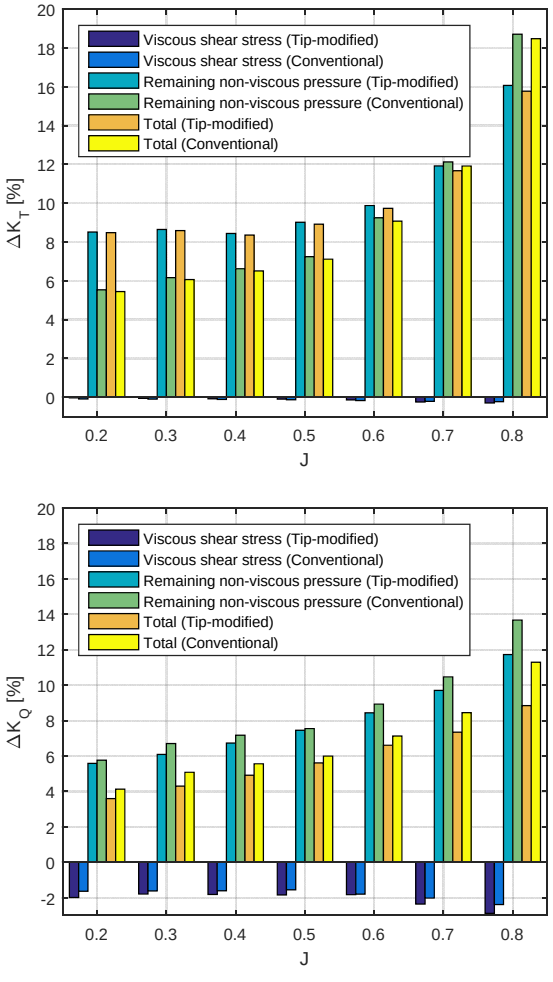

Figure 13: Differences of K_T and K_Q between model- and full-scale computations on tip-modified and conventional propellers ($\Delta\phi = \phi_{Full} / \phi_{Model} - 1$)

In Figure 13, the increases of K_T and K_Q from model to full scale are presented with portions from viscous shear stress and remaining pressure. The K_T increase is larger for the tip-modified propeller at the design condition and

high loadings of $J \leq 0.6$ and the difference of ΔK_T between the two propellers become larger at lower values of J, while ΔK_T is smaller for the tip-modified propeller at low loadings of $J \geq 0.7$. ΔK_Q is larger for the conventional propeller in the entire range of J and the difference of ΔK_Q is increased at high values of J. As ΔK_T is larger and ΔK_Q is smaller for the tip-modified propeller at the design condition and high loadings of $J \leq 0.6$, the difference of η_O between the two propellers becomes larger at full scale. At the design condition of $J = 0.6$, η_O is 1.6% higher for the tip-modified propeller at model scale, whereas the difference is increased to 2.7% at full scale. Both ΔK_T and ΔK_Q are larger for the conventional propeller at low loadings of $J \geq 0.7$, but the difference of ΔK_T is relatively larger than that of ΔK_Q and so η_O at full scale is higher for the conventional propeller at $J \geq 0.9$.

ΔK_T and ΔK_Q are mostly due to non-viscous pressure excluding viscous shear stress. The portions of K_T and K_Q from viscous shear stress are reduced at full scale, but the reduction is only within 0.3% for ΔK_T. The reduction of K_Q portion from viscous shear stress is 1.6 – 2.4%, which is relatively small compared to 5.6 -10.5% increase of the portion from remaining pressure.

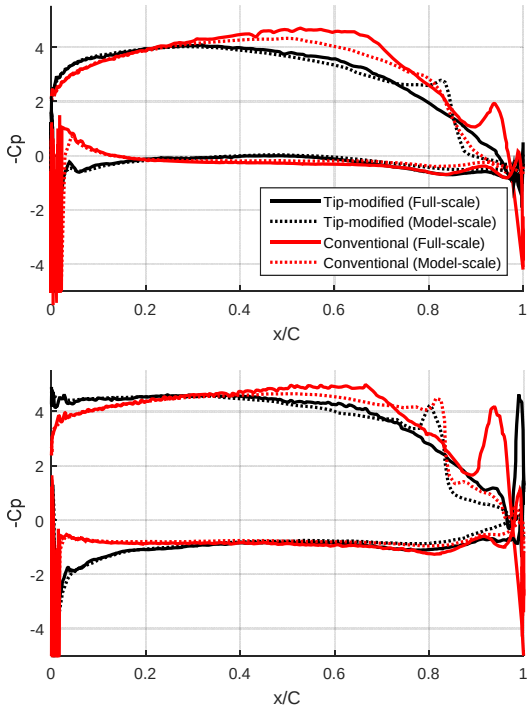

Figure 14: Sectional pressure distributions at 0.6R (top) and 0.8R (bottom) for the tip-modified and conventional propellers at model and full scale

The comparison of sectional pressure distributions between model and full scale in Figure 14 shows differences in the recovery pattern of the rooftop pressure on the suction side. While the rooftop pressure drops down with a high pressure gradient at $x/C = 0.8 – 0.9$ at model scale, it is recovered from $x/C \approx 0.7$ with a rather moderate pressure gradient at full scale. At full scale, pressure fluctuations indicating flow separations occur at $x/C = 0.9 – 0.95$ in the recovering process of the rooftop pressure for the conventional propeller, whereas such fluctuations are weak and confined to a small region near the trailing edge for the tip-modified propeller. As the spanwise blade loading is more distributed towards the tip for the tip-modified propeller, the circulation at the maximum loading region of $0.6R – 0.8R$ is 10.6 – 14.7% lowered compared to that for the conventional propeller. The comparison of the circulation distribution between the two propellers is found in Shin & Andersen (2016). The stronger flow separations related to the higher loading at $0.6R – 0.8R$ can lead to the efficiency loss of the conventional propeller.

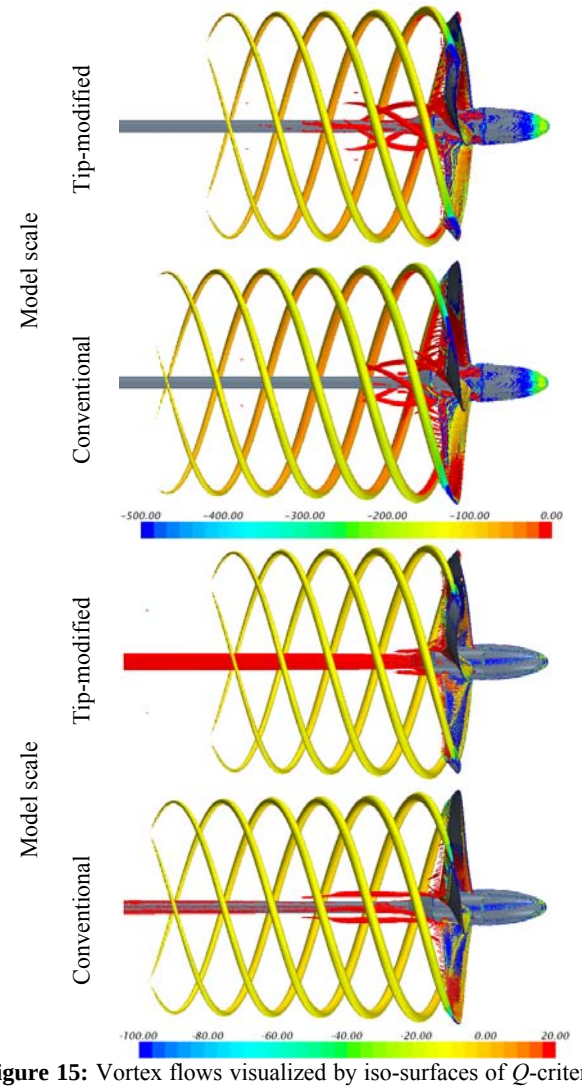

Figure 15: Vortex flows visualized by iso-surfaces of Q-criteria Q = 30,000 at model scale and Q = 240 at full scale with colors indicating the vorticity component around the axial direction

In Figure 15, the Q-criterion value for visualizing vortex flows at full scale is reduced more than 100 times from that at model scale so that the tip vortex extent normalized by the propeller diameter may be the same at both scales for the tip-modified propeller. The relative length of tip vortex is incomparable between model and full scale from iso-surfaces of an identical Q-criterion value mainly due to a higher propeller speed applied to the model-scale computations than that from Froude scaling. The tip vortex for the conventional propeller is slightly more

extended at full scale, which can bring additional efficiency loss on top of that at model scale.

Model-scale computations are repeated on both the propellers at a lower Rn from Froude scaling than that in the open-water model test. Computations at 3 intermediate scales between model and full scale are made with including the transition model. In Figure 16, the open-water efficiencies $\eta_{O,CTh}$ and $\eta_{O,KT}$ interpolated at the design thrust loading coefficient C_{Th} = 1.37 and the design thrust coefficient K_T = 0.20, respectively, are presented with respect to $Rn_{0.7}$. Both $\eta_{O,CTh}$ and $\eta_{O,KT}$ are increased and the increasing rates are gradually reduced at higher $Rn_{0.7}$. The overall increasing rate of $\eta_{O,CTh}$ is lower than that of $\eta_{O,KT}$ and the increase of $\eta_{O,CTh}$ for each propeller is within 0.5% at $Rn_{0.7} \geq 2.6 \cdot 10^6$.

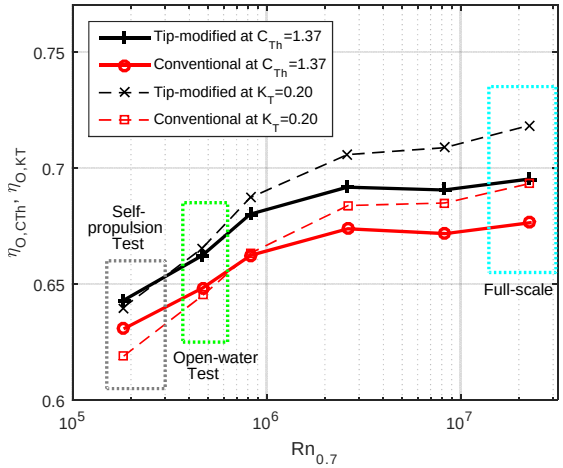

Figure 16: Open-water efficiencies at C_{Th} = 1.37 and K_T = 0.20 with varying the scale factor from model to full scale

The differences of $\eta_{O,CTh}$ and $\eta_{O,KT}$ between the two propellers are increased at higher $Rn_{0.7}$. While $\Delta\eta_{O,CTh}$ = 1.9% at $Rn_{0.7} = 1.8 \cdot 10^5$ is increased to 2.8% at $Rn_{0.7} = 2.3 \cdot 10^7$, $\Delta\eta_{O,KT}$ of 3.1 – 3.6% is larger than $\Delta\eta_{O,KT}$ at the entire range of $Rn_{0.7}$, but the variation of $\Delta\eta_{O,KT}$ from model to full scale is smaller, where $\Delta\eta = \eta_{Tip\text{-}modified} / \eta_{Conventional} - 1$. As the increase of the non-dimensionalized thrust at a certain value of J from model to full scale is larger for the tip-modified propeller, the difference of scale effects is more pronounced when considering $\eta_{O,CTh}$.

7 CONCLUSION

RANS computations have been made on tip-modified and conventional propellers at model and full scale. While a transition model is applied to the model scale computations, a fully turbulent flow is modeled in the full-scale computations without the transition model. Grid-independent solutions at model and full scale have been achieved by grid verification studies. The comparison of computations with and with the transition model shows that the effects of laminar and transitional flows are crucial for model-scale propellers.

The CFD analysis of scale effects shows that the increase of K_T from model to full scale is larger for the tip-modified propeller. The increase of K_Q is relatively smaller than that of K_T and the K_Q increase is larger for the conventional propeller, on the contrary. So the efficiency gain of the tip-modified propeller is increased at full scale. The scale effects are mostly due to non-viscous pressure excluding viscous shear stress. The larger scale effects of the tip-modified propeller in K_T and η_O are related to alterations of tip vortex and sectional pressure distributions by the bent tip and the higher spanwise loading at the tip region.

REFERENCES

Andersen, P., Friesch, J., Kappel, J. J., Lundegaard, L., & Patience, G. (2005). 'Development of a Marine Propeller with Nonplanar Lifting Surfaces'. Marine Technology **42**, No. 3.

Brown M., Sanchez-Caja, A., Adalid, J.G., Black, S., Sobrino, M. P., Duerr, P., Schroeder, S. & Saisto, I. (2014). 'Improving Propeller Efficiency Through Tip Loading'. Proc. of 30th Symp. on Naval Hydrodynamics, Hobart, Tasmania, Australia.

Bugalski, T., Streckwall, H. & Szantyr, J.A. (2013). 'Critical Review of Propeller Performance Scaling Methods Based on Model Experiments and Numerical Calculations'. Polish Maritime Research Vol.20, 4(80), pp.71-79.

Funeno, I. (2002). 'On Viscous Flow around Marine Propellers – Hub Vortex and Scale Effect'. Journal of Kansai Society of Naval Architects No. 238.

Haimov, H., Vicario, J. & Del-Corral, J. (2011). 'RANSE Code Application for Ducted and Endplate Propellers in Open Water'. Proc. of 2nd Intl. Symp. on Marine Propulsors SMP'11, Hamburg, Germany

ITTC. (2008) 'ITTC – Recommended Procedures and Guidelines: Performance, Propulsion 1978 ITTC Performance Prediction Method'. 25th ITTC

Krasilnikov, V., Sun, J., & Halse, K. H. (2009). 'CFD Investigation in Scale Effect on Propellers with Different Magnitude of Skew in Turbulent Flow'. Proc. of 1st Intl. Symp. on Marine Propulsors SMP'09, Tronheim, Norway

Sanchez-Caja, A., Gonzalez-Adalid, J., Perez-Sobrino, M., & Sipila, T. (2014). 'Scale Effects on Tip Loaded Propeller Performance Using a RANSE Solver'. Ocean Engineering **88**, pp.607-617.

Shin, K.W. & Andersen, P. (2016). 'CFD Study on Effective Wake of Conventional and Tip-modified Propellers'. Proc. of 31st Symp. on Naval Hydrodynamics, Monterey, CA, USA

Visonneau, G.B., Deng, G.B., Guilmineau, E., Queutey, P., & Wackers, J. (2016). 'Local and Global Assessment of the Flow around the Japan Bulk Carrier with and without Energy Saving Devices at Model and Full Scale'. Proc. of 31st Symp. on Naval Hydrodynamics, Monterey, CA, USA